Computer simulation of topological defects around a colloidal particle or droplet dispersed in a nematic host

Denis Andrienko,[1] Guido Germano,[1,2] and Michael P. Allen[1]
[1]*H. H. Wills Physics Laboratory, University of Bristol, Royal Fort, Tyndall Avenue, Bristol BS8 1TL, United Kingdom*
[2]*Theoretische Physik, Universität Bielefeld, 33501 Bielefeld, Germany*
(Received 6 November 2000; published 20 March 2001)

We use molecular dynamics to study the ordering of a nematic liquid crystal around a spherical particle or droplet. Homeotropic boundary conditions and strong anchoring create a hedgehog (radial point defect) director configuration on the particle surface and in its vicinity; this topological defect is canceled by nearby defect structures in the surrounding liquid crystal, so as to give a uniform director field at large distances. We observe three defect structures for different particle sizes: a quadrupolar one with a ring defect surrounding the particle in the equatorial plane; a dipolar one with a satellite defect at the north or south pole; and a transitional, nonequatorial, ring defect. These observations are broadly consistent with the predictions of the simplest elastic theory. By studying density and order-parameter maps, we are able to examine behavior near the particle surface, and in the disclination core region, where the elastic theory is inapplicable. Despite the relatively small scale of the inhomogeneities in our systems, the simple theory gives reasonably accurate predictions of the variation of defect position with particle size.

DOI: 10.1103/PhysRevE.63.041701 PACS number(s): 61.30.Cz, 61.30.Jf, 61.20.Ja, 07.05.Tp

I. INTRODUCTION

Suspensions of solid particles or immiscible liquid droplets in a host fluid (colloids) have attracted wide interest, due to a number of industrial applications (they appear in food, paints, ink, drugs) and fundamental research (they show features such as Casimir forces between the particles, formation of supermolecular structures, and novel phases). Colloidal systems with a *liquid crystal* as a host fluid are of special interest [1–3]. In the *nematic* liquid crystals considered here, while the system remains translationally disordered and liquidlike, there is long-range ordering of molecular orientations about a preferred direction, termed the *director*. Elastic deformations of the director field around the colloidal particles produce additional long-range forces between them. These interactions can be of dipolar or quadrupolar type depending on the symmetry of the director field around the particles [4], and this in turn is extremely sensitive to the *boundary conditions* on the particle surface and the size of the particles [5–7].

To understand the interaction between the particles, it is important to know the liquid crystal ordering near one single particle. This ordering is also important for calculation of the elastic light scattering from nematic emulsions [8]. The complication here is the presence of *topological defects* in such emulsions. Isolated drops provide a spherical confining geometry for the liquid crystal. Sufficiently strong homeotropic anchoring of the director (that is, normal to the particle surface) then induces a radial point (hedgehog) defect with topological charge $+1$. If the director field is uniform far from the particle, i.e., the total charge of the whole system is zero, topological considerations imply that an additional defect must be created in the medium to compensate the radial hedgehog.

There are several types of defect that can arise in this case. Two are illustrated in Fig. 1. The first is a hyperbolic hedgehog with a topological charge -1, called a dipolar or *satellite* defect. The second is a quadrupolar or *Saturn-ring* defect, i.e., a $-1/2$ strength disclination ring that encircles the spherical particle. Theoretical and numerical work based on the elastic theory [9,10] suggests that the dipole configuration is stable for the micrometer-sized droplets that are usually realized experimentally; the Saturn-ring configuration should appear if the droplet size is reduced and, when present, it is always predicted to be most stable in the equatorial plane normal to the director. If the strength of the surface anchoring is weak enough, a third, *surface-ring*, director configuration is possible [5,10]. It has also been found that the *twisted dipole* configuration is possible for high enough ratios of twist to splay elastic constants [10].

However, the elastic theory has several disadvantages because of the way it treats the core structure of the defect embedded into the nematic host. First, the defect core region is considered as an isotropic inclusion with some unknown free energy which is used as an adjustable parameter of the theory. Second, the liquid crystalline phase is treated as uniaxial. However, near the defect core (or indeed the particle surface) these assumptions are no longer valid. As has already been demonstrated [11–14], the defect core of the simplest disclination line of strength $+1$ has a rather com-

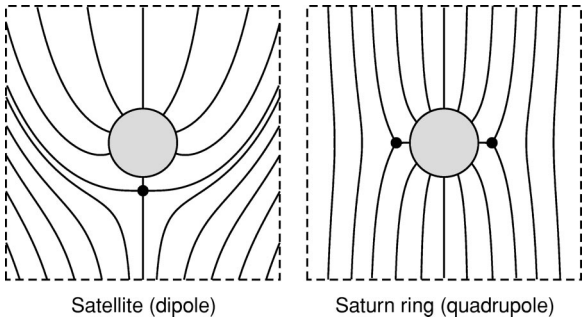

FIG. 1. Sketches of the satellite defect and Saturn-ring defect.

plex structure: the order parameter varies near the core region; the uniaxial phase becomes biaxial; even the density of the mesophase can be affected by the presence of the wall or the defect [14,15].

For a better description it is necessary to use the full order-parameter tensor to describe liquid crystalline ordering [16–18]. This tensor exhibits no anomalous behavior at the singularity of the director field. Moreover, one can resolve order-parameter variation as well as biaxiality of the defect core using a Landau–de Gennes phenomenological expansion of the free energy. In this framework, only the liquid crystal density is assumed to be fixed. In its turn, density variation can be taken into account using Onsager theory [15], although that approach will not be pursued here.

Another approach to the study of defect core structure is to use computer simulation. Indeed, computer simulation is a well established method to treat bulk elastic coefficients [19,20], the surface anchoring strength [15,21], and structures of disclination cores [14,22]. This means that computer simulation allows one to investigate the details of liquid crystalline structure that are difficult to resolve experimentally or using phenomenological theories, e.g., density variation, biaxiality of the mesophase near the defect core, etc.

In this paper we present the results of molecular dynamics (MD) simulations of the topological defects that appear in the liquid crystalline mesophase around a spherical droplet or colloid particle. Our study complements previous results obtained by Billeter and Pelcovits [23], who used systems of 2048 molecules modeled by the Gay-Berne potential. The present study investigates the effect of changing the droplet size, and uses much larger numbers of molecules, up to one million. This turns out to be essential to avoid finite-size effects which are particularly important for the satellite defect, since it causes long-range director deformation. As well as observing both the Saturn-ring and satellite defects, with the latter being stable only for larger particle sizes as expected, we also observe a transition between these two structures involving an intermediate, nonequatorial, surface-ring defect.

The paper is organized as follows. In Sec. II we present the computational details and molecular models we use to simulate the liquid crystal mesophase and the interaction of the molecules with the droplet surface. Section III contains the results of the simulations: density, director, order-parameter, and biaxiality profiles for the Saturn-ring, satellite, and surface-ring defects. We also compare our results to the known predictions of the elastic theory. Concluding remarks are given in Sec. IV.

II. MOLECULAR MODEL AND SIMULATION METHODS

Molecular dynamics simulations were carried out using axially symmetric molecules interacting through the pair potential

$$v_{ij}=\begin{cases} 4\varepsilon_0(\varrho_{ij}^{-12}-\varrho_{ij}^{-6})+\varepsilon_0, & \varrho_{ij}^6<2 \\ 0, & \varrho_{ij}^6>2. \end{cases} \qquad (1)$$

TABLE I. Run parameters

Colloid radius R	Number of particles N	Defect type	Run length (steps)
3	8 000	Saturn ring	1 500 000
5	8 000	Saturn ring	1 500 000
6	8 000	Saturn ring	1 500 000
7	8 000	Saturn ring	1 500 000
10	64 000	Saturn ring	500 000
10	64 000	off-center ring	1 000 000
15	1 000 000	Saturn ring	500 000
15	1 000 000	satellite	500 000

Here $\varrho_{ij}=(r_{ij}-\sigma_{ij}+\sigma_0)/\sigma_0$; r_{ij} is the center-center separation, σ_0 a size parameter, ε_0 an energy parameter (both taken to be unity), and the orientation-dependent diameter σ_{ij} is defined by

$$\sigma_{ij}=\sigma_0\left\{1-\frac{\chi}{2}\left[\frac{(\hat{\mathbf{r}}_{ij}\cdot\hat{\mathbf{u}}_i+\hat{\mathbf{r}}_{ij}\cdot\hat{\mathbf{u}}_j)^2}{1+\chi(\hat{\mathbf{u}}_i\cdot\hat{\mathbf{u}}_j)}+\frac{(\hat{\mathbf{r}}_{ij}\cdot\hat{\mathbf{u}}_i-\hat{\mathbf{r}}_{ij}\cdot\hat{\mathbf{u}}_j)^2}{1-\chi(\hat{\mathbf{u}}_i\cdot\hat{\mathbf{u}}_j)}\right]\right\}^{-1/2}$$

where $\chi=(\kappa^2-1)/(\kappa^2+1)$, κ being the elongation. In this work we used $\kappa=3$ throughout. The orientation dependence is written in terms of the direction of the center-center vector $\hat{\mathbf{r}}_{ij}=\mathbf{r}_{ij}/r_{ij}$ and the unit vectors $\hat{\mathbf{u}}_i$, $\hat{\mathbf{u}}_j$ which specify the molecular symmetry axes. This is a soft repulsive potential, describing (approximately) ellipsoidal molecules; it may be thought of as a variant of the standard Gay-Berne potential [24,25] with exponents $\mu=0,\nu=0$. The molecular mass m was taken to be unity, and the molecular moment of inertia fixed as $I=2.5m\sigma_0^2$.

The interaction of molecule i with the droplet was given by a shifted Lennard-Jones repulsion potential between the centers, having exactly the same form as Eq. (1), but with ϱ_{ij} replaced by $\varrho_i=(|\mathbf{r}_i-\mathbf{r}_c|-\sigma_c+\sigma_0)/\sigma_0$ and $\sigma_c=R+\sigma_0/2$. Here, R is the colloid radius, and $\mathbf{r}_c$ the position of the colloid center. This interaction potential results in homeotropic anchoring of the liquid crystal molecules, normal to the particle surface.

The systems consisted of $N=8000$–$1\,000\,000$ particles depending on the droplet radius (in the range $R/\sigma_0=3$–15) and defect type: details appear in Table I. A molecular dynamics program was run on a Cray T3E using a domain decomposition algorithm [26]. A reduced temperature $k_BT/\varepsilon_0=1$ was used throughout (for this model, the phase behavior is not sensitively dependent on temperature, as there are no attractive forces). The system size was chosen so that the number density of the liquid crystal far from the colloid was $\rho\sigma_0^3=0.35$, which lies well within the nematic region, with a corresponding bulk order parameter $S\approx0.81$. For this system, in the reduced units defined by σ_0, ε_0, and m, a time step $\delta t=0.004$ was found suitable.

Cubic periodic boundary conditions were employed in all the simulations. To facilitate the analysis, the position of the droplet was fixed in the center of the simulation box, and a global constraint was applied to fix the orientation of the director along the z axis [27].

To obtain the particular defect types of interest we have used several methods to prepare the initial configuration.

(1) The radius of the colloid droplet was steadily increased from a small value in systems that were already in the nematic state. This takes about 10^4 steps to increase the droplet radius up to $R/\sigma_0=10$ and about 10^4 steps to equilibrate the system with the defect. This method generates an energetically favorable configuration of the kind that is stable for small colloid particles (i.e., the ring defect).

(2) Disordered, isotropic configurations containing the colloid droplet were compressed to the ordered, nematic state. This method, in principle, should give the lowest free-energy configurations in an unbiased way. However, for large systems, equilibration from the isotropic phase is extremely time consuming: systems split into small domains which then realign (coarsen).

(3) For large systems, we prepared director configurations in the nematic state with the defect embedded in them. To introduce the defect into the mesophase we used approximate analytical expressions for the director field $\mathbf{n}(\mathbf{r})$ around the droplet, which were used to determine the initial molecular orientations. This configuration was diluted, i.e., the molecule coordinates were scaled so that they did not overlap with each other or the colloid droplet. We compressed the system under low temperature ($T=0.1$) to the desired density. The low-temperature compression preserves the director structure in the system. Therefore, the original defect structure is still present in the system after the compression. After the compression, the system was equilibrated for 10^5 steps. This method allows one to prepare and observe metastable configurations, i.e., those that are local minima of the system free energy.

III. SIMULATION RESULTS AND DISCUSSION

Simulation results were analyzed to give director, density, order-parameter, and biaxiality maps. The coordinate systems used to describe positional and orientational variables are shown in Fig. 2. Positions, relative to the colloid particle at the origin, are expressed in spherical polar coordinates (r,θ,ϕ); the system was assumed to be invariant to rotations about the z axis. Accordingly, all quantities were averaged over angle ϕ (by rotating molecular positions and orientations together) before accumulating simulation averages on a grid with $\Delta r=(0.05\text{–}0.1)\sigma_0$, $\Delta\theta=10°$. At each grid point, the order tensor $\mathbf{Q}$ was resolved into components based on cylindrical polar unit vectors, pointing (i) along the z axis $\hat{\mathbf{z}}$, (ii) in the direction $\hat{\mathbf{e}}_\rho$ of increasing distance $\rho=\sqrt{x^2+y^2}$ from the z axis, and (iii) in the tangential direction $\hat{\mathbf{e}}_\phi=\hat{\mathbf{z}}\times\hat{\mathbf{e}}_\rho$:

$$Q_{\alpha\beta}(r_i,\theta_j)=\frac{1}{n_{\{i,j\}}}\sum_{k=1}^{n_{\{i,j\}}}\left\{\frac{3}{2}\langle u_{k\alpha}u_{k\beta}\rangle-\frac{1}{2}\delta_{\alpha\beta}\right\},$$

$$\alpha,\beta=\rho,\phi,z, \tag{2}$$

where there are $n_{\{i,j\}}$ molecules present in the bin $\{i,j\}$, $\delta_{\alpha\beta}$ is the Kronecker delta, and $\langle\cdots\rangle$ denotes an ensemble average. Diagonalizing this tensor, for each bin, gives three eigenvalues and three corresponding eigenvectors. The largest eigenvalue defines the order parameter $S(r,\theta)$ for each bin. The biaxiality α is defined as

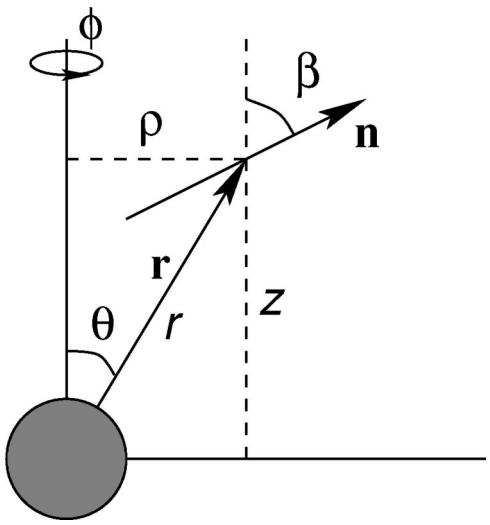

FIG. 2. Coordinate systems used in this work. The system is assumed to have rotational symmetry about the z axis. The director field is assumed to have axial ($\hat{\mathbf{z}}$) and radial ($\hat{\mathbf{e}}_\rho$) components only, and so may be described by the angle $\beta(r,\theta)$.

$$\alpha=\frac{1}{3}(S_2-S_3), \tag{3}$$

where S_2,S_3 are the two remaining eigenvalues of the averaged order tensor $\mathbf{Q}$ [11].

A. Ring defect

For all studied radii ($R/\sigma_0=3\text{–}15$) the ring defect appears immediately after equilibration of the system starting from the isotropic state or on expanding the droplet in the nematic state. We therefore concluded that this type of defect is energetically more favorable for the chosen droplet sizes. For large configurations, we also used the method with the predefined director field. In the case of the ring defect, we used the trial function for the director angle (see Fig. 2)

$$\beta(r,\theta)=\arccos[n_z(r,\theta)]$$

proposed by Kuksenok *et al.* [5,6]. This trial function captures the far-field behavior and a ring of $(-1/2)$ singularity at $r=a_r$, $\theta=\pi/2$:

$$\beta(r,\theta)=\theta-\frac{1}{2}\arctan\frac{\sin 2\,\theta}{1/f(r)+\cos 2\,\theta}. \tag{4}$$

Here $f(r)$ is a unique function of r and independent of the angle θ. $f(r)$ has also to comply with the boundary conditions: $1/f(\infty)=0(\Rightarrow\beta=0)$ far from the particle and $f(R)=0(\Rightarrow\beta=\theta)$ on the particle surface.The explicit form of the function $f(r)$ can be found in Refs. [5,6].

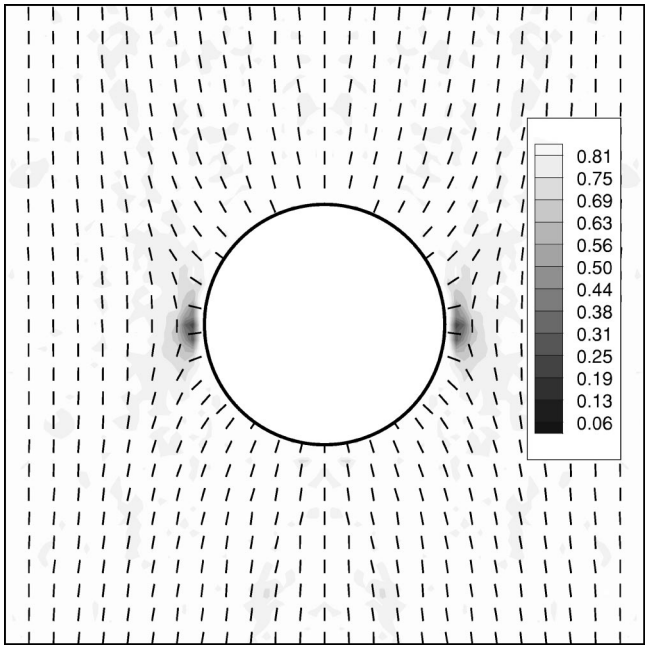

FIG. 3. Director map of the ring defect. Droplet radius $R=15$. The shading represents the value of the order parameter. The defect core is located close to the droplet surface, $a_r \approx 1.164R$. The director variation rapidly vanishes in the cell bulk.

A typical director map of the ring defect obtained from the simulations is shown in Fig. 3. From this map one can see that the ring defect does not have long-range director distortions. Its core region is located very close to the droplet surface and the director distortion vanishes very quickly in the liquid crystal bulk. This is in agreement with the *quadrupolar* nature of the defect: far from the particle the director deviation angle has asymptotic behavior $\beta \sim (R/r)^3 \sin 2\theta$. Therefore, this type of defect can be studied using a comparatively small number of particles and correspondingly small simulation boxes (see Table I for details).

Typical density profiles for the ring defect with $R=15$ are shown in Fig. 4 for $\theta=0,\pi$ (not intersecting the defect) and $\theta=\pi/2$ (crossing the disclination ring). The profiles that avoid the disclination have an oscillating structure near the particle surface that is typical for a *liquid-wall* interface. The profiles that cross the disclination ring do not have oscillations. The difference may be due to the partial melting of the liquid crystal in the disclination core region. This melting damps the influence of the droplet surface on the interface region. Note that, even though the disclination core is located close to the particle surface, the region where the density has an oscillating structure is quite big. Therefore, the simulation box has to be of adequate size in order not to affect the defect structure.

The order-parameter profiles for $\theta=0,\pi/2$ are shown in Fig. 5. The shape of these profiles in general reflects the typical structure of the core: the center of the core has lower order than the bulk and the core region extends over a few molecular lengths. Using order-parameter profiles one can also define the position of the disclination ring as the location of the minimum of the order parameter. For large

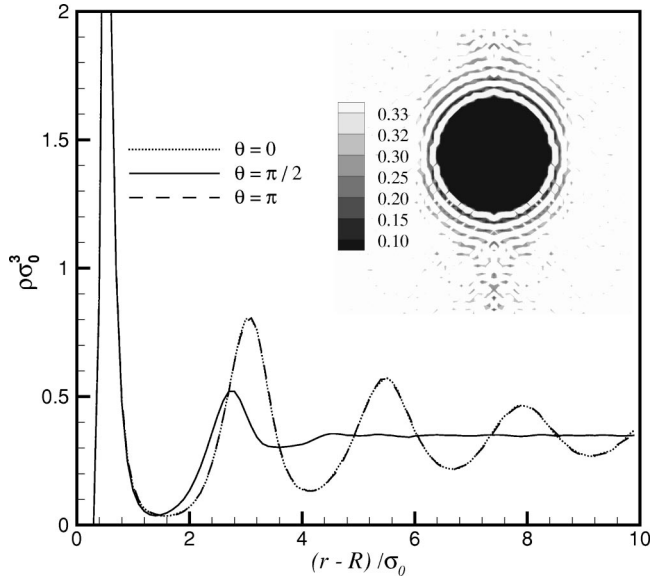

FIG. 4. Density profiles for the ring defect. We plot dimensionless number density $\rho\sigma_0^3$ versus reduced distance r/σ_0. Droplet radius $R/\sigma_0=15$. The following directions are shown: $\theta=0,\pi$ (avoiding the defect) and $\theta=\pi/2$ (crossing the disclination ring). The inset shows the contour plot of the density map.

enough R a second minimum appears, indicating that the disclination ring defect has a complex structure. This minimum is probably due to the density modulation near the droplet surface. As we will see, the density modulation also influences the rest of the profiles.

To emphasise the complex structure of the defect core we plot the biaxiality profiles (Fig. 6). From the order and biaxiality profiles one can see that the main biaxial ring is accompanied by one additional biaxial ring for large R, or even two extra rings for some R (e.g., $R/\sigma_0=5,6$). Again, this is most likely due to the density modulation near the droplet surface.

Using the minima of the order profiles (or, with the same results, the maxima of the biaxiality profiles) we extracted

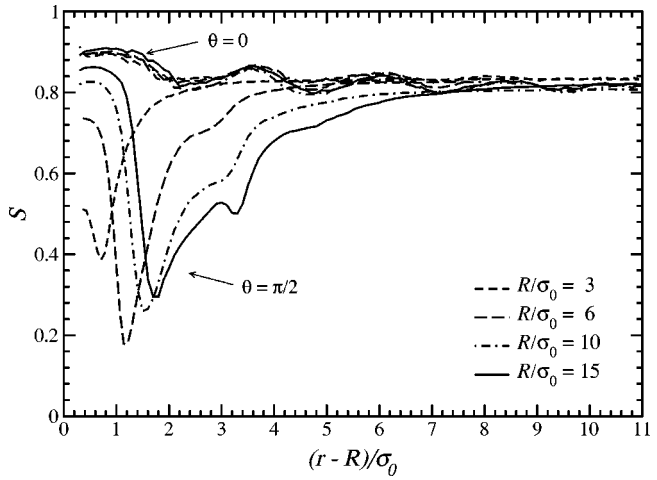

FIG. 5. Order-parameter profiles for the ring defect along the directions $\theta=0,\pi/2$. Different curves correspond to different droplet radii. The minimum of the order parameter defines the position of the disclination core.

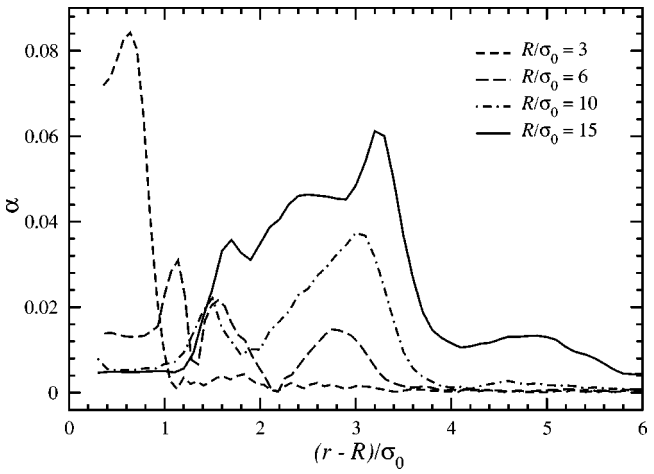

FIG. 6. Biaxiality profiles along the direction $\theta=\pi/2$ (across the defect). We plot the biaxiality parameter α versus reduced distance r/σ_0. The peak of the biaxiality is centered on the defect core and coincides with the minimum of the order parameter (Fig. 5).

the distance from the core of the disclination ring to the particle surface. The dependence of this distance on the particle radius R is shown in Fig. 7. It is interesting to compare with the phenomenological theory predicting linear dependence of the ring defect radius on the droplet radius: $a_r \approx 1.25R$ from minimization of the elastic free energy using a trial function [5], $a_r \approx 1.13R$ using a simulated annealing method [9], or $a_r \approx 1.26R$ [10]. Our MD simulation results give $a_r - R = -0.33\sigma_0 + (0.164 \pm 0.004)R$, which is in good agreement with the phenomenological theory, especially if one bears in mind the complex structure of the defect core.

B. Satellite defect

The director field around the satellite defect is illustrated in Fig. 8. The director distortion extends much further than that of the ring defect. This is a direct consequence of the symmetry of the director distribution of the satellite defect:

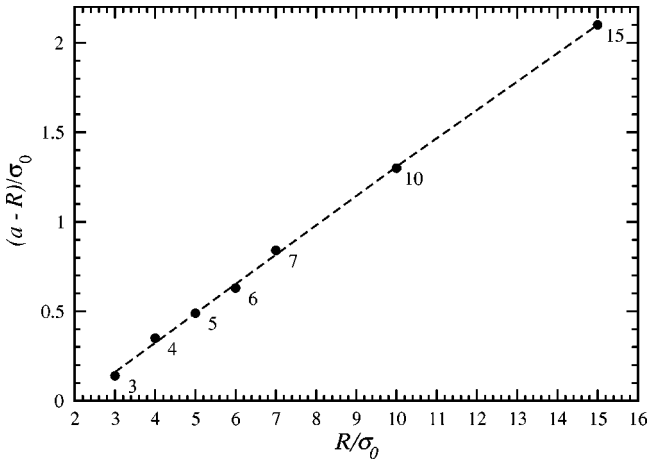

FIG. 7. Distance of the core region of the ring defect from the droplet center, as a function of reduced droplet radius R/σ_0. We also show the linear fit to the simulation results, $a_r = 1.164R - 0.33\sigma_0$.

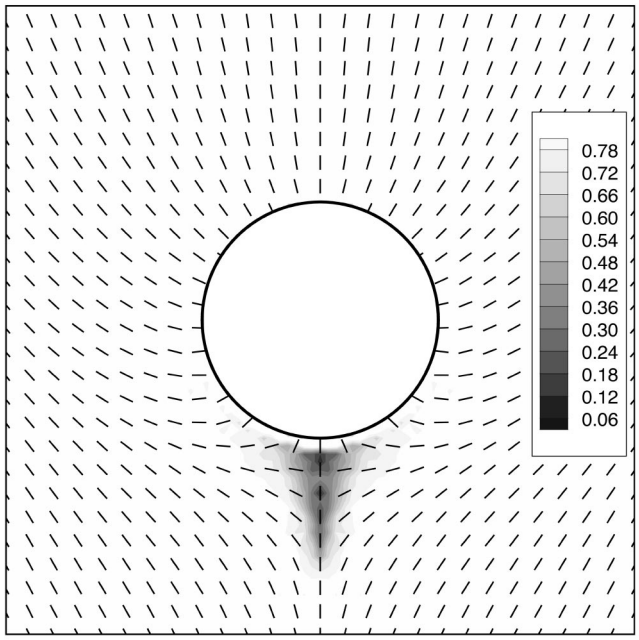

FIG. 8. Director map of the satellite defect. Droplet radius $R/\sigma_0 = 15$. The background contour plot represents the value of the order parameter.

far from the particle, the director angle vanishes as $\beta \sim (R/r)^2 \sin\theta$, i.e., it is like a dipolar term in a multipole expansion. Therefore, to study the satellite defect, one needs very large systems. We used one million particles and droplet radius $R=15$.

The approach involving a trial function was used to generate the dipolar initial configuration, as in the case of the Saturn ring. In this case superposition of the radial and hyperbolic hedgehogs implies the following ansatz [6]:

$$\beta(r,\theta) = \theta - \arctan\frac{\sin\theta}{1/f(r) + \cos\theta}. \tag{5}$$

Again, $f(r)$ is supposed to be a unique function of r which does not depend on the angle θ. The boundary condition now is $1/f(\infty)=0$ $(\Rightarrow \beta = 0)$ far from the particle; the position of the hyperbolic hedgehog is defined by $f(a_s)=1$. After the initial configuration was generated the system was equilibrated for 50 000 steps with the subsequent production runs extending to 500 000 steps.

The density profiles for the satellite defect are shown in Fig. 9. The following directions are shown: $\theta=\pi$ (through the defect) and $\theta = 0, \pi/2$ (avoiding the defect). One can see that the density profile at $\theta=\pi$ (across the defect core) has a less prominent oscillating structure than the other two: this is again presumably due to the partial disordering of the mesophase in the core region.

The order-parameter profiles for $\theta = 0, \pi/2, \pi$ are shown in Fig. 10. One can see that the defect core region is quite elongated with its long axis parallel to the far-field director. It is difficult to judge the position of the satellite defect from the order-parameter profiles: the region occupied by the disclination core is rather large. The same comment applies to

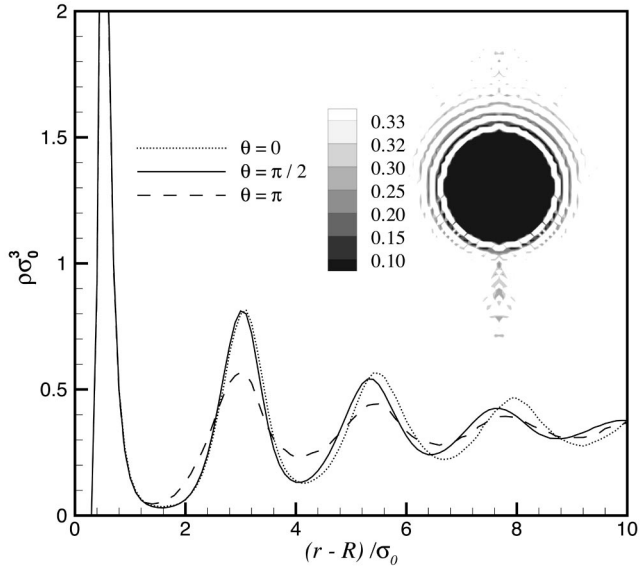

FIG. 9. Density profiles for the satellite defect. Droplet radius $R/\sigma_0=15$. The following directions are shown: $\theta=0,\pi/2$ (both avoiding the defect) and $\theta=\pi$ (crossing the defect). The contour plot of the density map is shown in the inset.

the biaxiality profiles shown in Fig. 11. Again, as in the case of the ring defect, both order-parameter and biaxility profiles are affected by the density oscillations near the particle surface.

By examining the director field lines in Fig. 8 one can estimate that the center of the defect core is located at a distance $a_s \approx 1.4R$. The value predicted by the elastic theory is about $1.22R$ for the simulated annealing calculations [9]; $1.17R$ [1] or $1.46R$ [6] for the free-energy minimization using a trial function.

C. Off-center ring

Simulation results show that both the satellite and ring defects are at least metastable for $R/\sigma_0=15$: once the particular defect is realized in the system, it is stable over the time scale that is accessible to our simulations. However, the satellite defect is not stable for the smaller droplets. Indeed, we observed a rapid transition (several thousands of MD steps) of the satellite defect to the ring defect for $R/\sigma_0<10$. Equilibrating the initial configuration with the satellite defect in the cell with droplet radius $R/\sigma_0=10$, we observed that it evolves into an *off-centered* ring defect: a typical nematic director map is shown in Fig. 12. The ring moved slowly, evolving toward an equatorial Saturn-ring configuration. From long runs (up to a million time steps) we conclude that

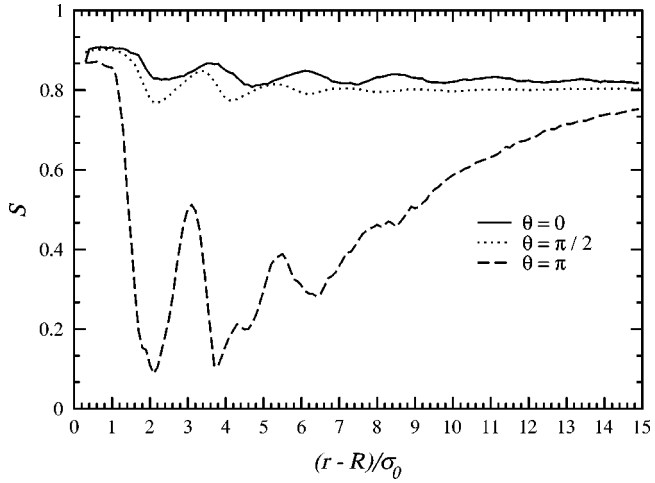

FIG. 10. Order-parameter profiles for the satellite defect along the directions $\theta=0,\pi/2,\pi$. Droplet radius $R/\sigma_0=15$. The defect core is elongated with the long axis parallel to the far-field director.

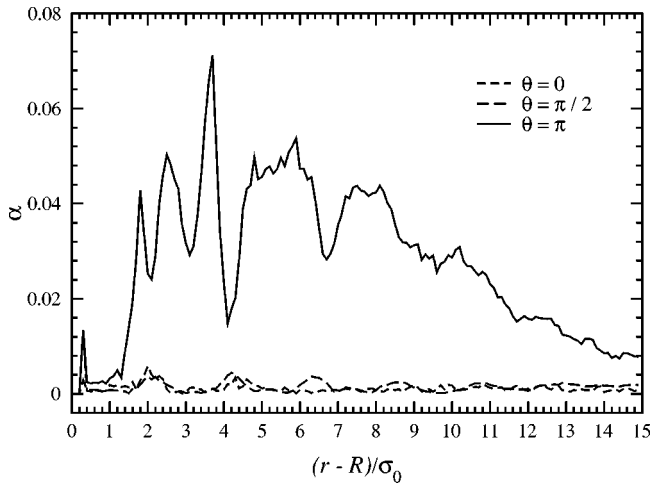

FIG. 11. Biaxiality profiles for the satellite defect ($\theta=0,\pi/2,\pi$). Droplet radius $R=15$. From these profiles one can define the center of the satellite defect as a maximum of the biaxiality. The small blip close to the droplet surface is due to the surface effects: it is seen on all profiles.

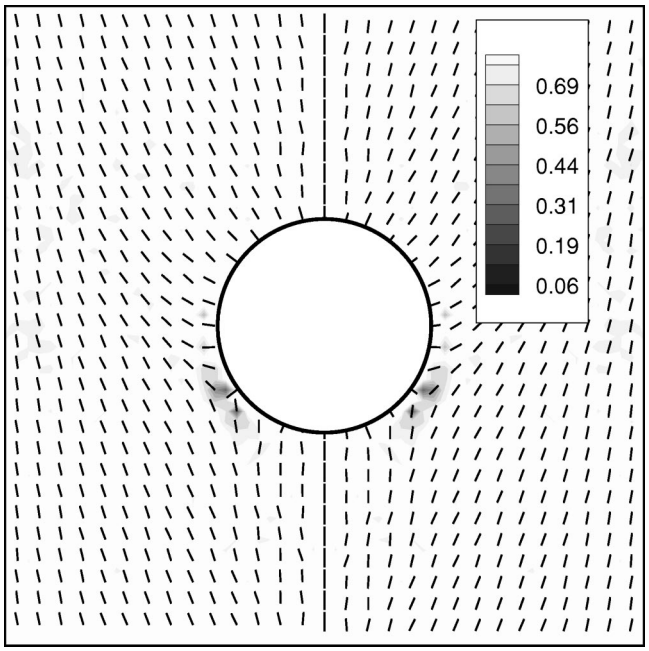

FIG. 12. Director map for the off-center ring configuration. The background contour plot represents the value of the order parameter.

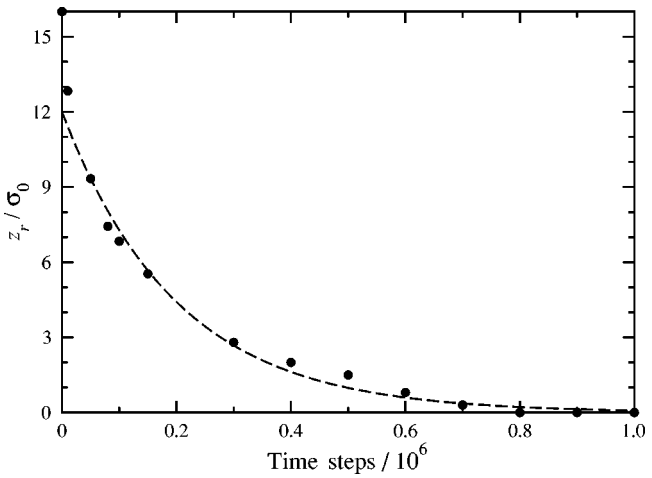

FIG. 13. Dynamics of the transition from the satellite defect to the Saturn-ring defect via an off-center ring configuration. We plot the z coordinate of the ring defect relative to the droplet center, versus the number of time steps. As a guide, the dashed line corresponds to exponential decay with a time constant of 2×10^5 time steps.

this is an intermediate state between the satellite and the Saturn-ring defects. The z coordinate of the ring relative to the droplet center as a function of the number of time steps, is shown in Fig. 13. The evolution dynamics is quite slow. In principle, one might observe the same type of transition in the opposite direction, for droplet sizes large enough to stabilize the satellite defect; this is still unreachable for the system sizes we explore here. Note that elastic theory also predicts the off-center ring configuration to be unstable [10], with the transition from the dipole configuration to the Saturn-ring configuration occurring via this intermediate state.

IV. CONCLUSIONS

We used molecular dynamics to study a spherical object, representing a small colloidal particle or droplet, suspended in a nematic liquid crystal matrix modeled with the soft ellipsoidal potential. Homeotropic boundary conditions and strong anchoring create a hedgehog director configuration on the particle surface and in its vicinity; we have studied the defect structure around the particle that cancels this hedgehog defect and produces a uniform director field at large distances. We investigated systems up to 10^6 particles with a domain decomposition program on a massively parallel computer, conducting runs of up to 1.5×10^6 time steps.

Our simulation results show that, in the case of a small droplet, only a Saturn-ring defect is stable; an initial configuration containing a satellite defect evolves spontaneously into a ring. For large enough droplets, however, both the satellite and the ring defect are at least metastable on the time scale of the simulations. For intermediate sizes of colloid particle, a nonequatorial surface ring evolves very slowly toward the Saturn-ring configuration.

Using order-parameter maps we are able to resolve the position of the core of the defect; these also show that the nematic phase is strongly biaxial near the defect core. In these systems, the defect region is quite large: in some cases of a similar size to the colloid particle itself. Far from the particle the director profiles are in good agreement with those predicted by elastic theory. The elastic theory also predicts quite well the variation of defect position with colloid particle radius.

It should be borne in mind that the colloid dimensions studied here are much smaller than those typically investigated experimentally; indeed, it is quite surprising that the satellite defect is observable in our simulations, and that the off-center surface ring, which is never seen as a stable configuration in the elastic theory, appears, albeit as a transition state. It is hoped that further work, aimed at estimating free-energy differences between these structures, will clarify the situation.

ACKNOWLEDGMENTS

This research was supported by EPSRC Grant Nos. GR/L89990 and GR/M16023, and through INTAS Grant No. 99-00312. D.A. acknowledges support from the Overseas Research Students Program; G.G. acknowledges the support of the British Council; M.P.A. is grateful to the Alexander von Humboldt Foundation and the Leverhulme Trust.

[1] P. Poulin, H. Stark, T.C. Lubensky, and D.A. Weitz, Science **275**, 1770 (1997).
[2] P. Poulin and D.A. Weitz, Phys. Rev. E **57**, 626 (1998).
[3] B.I. Lev and P.M. Tomchuk, Phys. Rev. E **59**, 591 (1999).
[4] T.C. Lubensky, D. Pettey, N. Currier, and H. Stark, Phys. Rev. E **57**, 610 (1998).
[5] O.V. Kuksenok, R.W. Ruhwandl, S.V. Shiyanovskii, and E.M. Terentjev, Phys. Rev. E **54**, 5198 (1996).
[6] S.V. Shiyanovskii and O.V. Kuksenok, Mol. Cryst. Liq. Cryst. Sci. Technol., Sect. A **321**, 489 (1998).
[7] O. Mondain-Monval, J.C. Dedieu, T. Gulik-Krzywicki, and P. Poulin, Eur. Phys. J. B **12**, 167 (1999).
[8] M. Lednei, I. Pinkevich, and V. Reshetnyak, Mol. Cryst. Liq. Cryst. Sci. Technol., Sect. A **331**, 2461 (1999).
[9] R.W. Ruhwandl and E.M. Terentjev, Phys. Rev. E **56**, 5561 (1997).
[10] H. Stark, Eur. Phys. J. B **10**, 311 (1999).
[11] P. Biscari and E.G. Virga, Int. J. Non-Linear Mech. **32**, 337 (1997).
[12] N.J. Mottram and S.J. Hogan, Philos. Trans. R. Soc. London, Ser. A **355**, 2045 (1997).
[13] I. Sigillo, F. Greco, and G. Marrucci, Liq. Cryst. **24**, 419 (1998).
[14] D. Andrienko and M.P. Allen, Phys. Rev. E **61**, 504 (2000).
[15] M.P. Allen, Mol. Phys. **96**, 1391 (1999).
[16] A. Sonnet, A. Kilian, and S. Hess, Phys. Rev. E **52**, 718 (1995).
[17] N. Schopohl and T.J. Sluckin, Phys. Rev. Lett. **59**, 2582 (1987).

[18] N. Schopohl, Phys. Rev. Lett. **60**, 755 (1988).
[19] M.P. Allen and D. Frenkel, Phys. Rev. A **37**, 1813 (1988).
[20] M.P. Allen and D. Frenkel, Phys. Rev. A **42**, 3641(E) (1990).
[21] D. Andrienko, G. Germano, and M.P. Allen, Phys. Rev. E **62**, 6688 (2000).
[22] S.D. Hudson and R.G. Larson, Phys. Rev. Lett. **70**, 2916 (1993).
[23] J.L. Billeter and R.A. Pelcovits, Phys. Rev. E **62**, 711 (2000).
[24] B.J. Berne and P. Pechukas, J. Chem. Phys. **56**, 4213 (1972).
[25] J.G. Gay and B.J. Berne, J. Chem. Phys. **74**, 3316 (1981).
[26] M.R. Wilson, M.P. Allen, M.A. Warren, A. Sauron, and W. Smith, J. Comput. Chem. **18**, 478 (1997).
[27] G. Germano (unpublished).